

Influence of alternative fuels on the particulate matter micro and nano-structures, volatility and oxidation reactivity in a compression ignition engine

Dongxu Mao ^{a,b}, Meisam Ahmadi Ghadikolaei ^{b,c,*}, Chun Shun Cheung ^b, Zhaojie Shen ^a, Wenzheng Cui ^a, Pak Kin Wong ^c

^a School of Automotive Engineering, Harbin Institute of Technology, Weihai, 2642209, China

^b Department of Mechanical Engineering, The Hong Kong Polytechnic University, Hung Hom, Kowloon, Hong Kong

^c Department of Electromechanical Engineering, University of Macau, Taipa, Macau



ARTICLE INFO

Keywords:

Alcohol fuel
Alternative fuel
Diesel engine
PM oxidation reactivity
PM structure
Ternary fuel

ABSTRACT

The present study investigates the impact of various alternative fuels, including biodiesel, methanol, ethanol, butanol and pentanol, on the micro and nano-structures, volatility and oxidation reactivity of particulate matter (PM) from a 4-cylinder compression ignition engine under low (10%) and high (80%) engine loads at a constant engine speed of 1800 rpm. Four alcohols were mixed with diesel and biodiesel to obtain ternary fuels. The overall oxygen concentration of each ternary fuel was fixed at 6% by mass for establishing the same condition for comparing. In addition to the ternary fuels, pure biodiesel was also compared with diesel fuel. The results of the micro and nano-structures characteristics obtained from a Scanning Transmission Electron Microscope (STEM) reveal that the alternative fuels can disorder the PM micro and nano-structures, and also the particles produced by these fuels have lower primary particle diameter, particle agglomerate size and fringe length, however, higher fringe tortuosity and almost equal (insignificant rise) fringe separation distance compared to those produced by diesel fuel. The results obtained from a Thermogravimetric Analyzer/Differential Scanning Calorimeter (TGA/DSC) show that both biodiesel and alcohols have the potential to increase in PM volatile substances and oxidation reactivity rate, and decrease in PM non-volatile substances in comparison with those of diesel fuel. It is concluded that the pure biodiesel has the highest impact on the PM structure, volatility and oxidation reactivity among all the tested alternative fuels, while methanol has the highest impact on these parameters among all the tested alcohol fuels.

1. Introduction

The compression ignition (CI) engine is one of the main origins of fine particulate matter (PM) in the atmosphere [1,2]. The PM produced by the CI engines causes different effects on human health and the environment due to its different physicochemical properties [3–7]. The diesel PM is composed of microscopic particles. In addition, it consists of non-volatile (soot) and volatile (adsorbed hydrocarbons) substances. The differences in the size, structure and volatility of diesel PM from different CI engines at different operating conditions have impacts on the oxidation properties of the PM, while they are essential parameters which need to be considered for designing of the after-treatment systems for the oxidation of PM. Thus, the formation mechanism and control

technology of diesel PM have become a research hotspot in the related fields.

Many scholars have conducted various studies on the structure (both micro and nano-structures), volatility and oxidation reactivity of diesel PM. Lee et al. [8] used an electron microscope to observe the PM micro-structure from a turbocharged CI engine. They found that the diesel PM consisted of some chain-like particles, and the structure of the particles varied significantly as the engine load was changed. Wal and Tomasek [9] used a transmission electron microscope (TEM) for understanding the carbonization process of flame soot precursors. They found that the soot was transparent in the lower flame zone, while in the higher flame zone, the soot had a bigger size, the formation of obvious boundaries also could be seen. In addition, they also defined the

* Corresponding author.

E-mail address: meisam.ahmadi67@yahoo.com (M.A. Ghadikolaei).

nano-structure characteristic parameters such as crystallite size, layer spacing, and curvature. Lu et al. [10] explored the influence of various engine loads on the PM micro-structure. They found that the microscopic size of the PM increased with the increase of the load, and the smaller initial particles collided and polymerized to form larger particulate matter. They also found that the engine load had significant impacts on the particle nano-structure parameters.

Several studies have confirmed that the PM microphysical and chemical characteristics from CI engines are decisive factors for determining the oxidation reactivity of PM [11,12]. It is found that the oxidation reactivity of the particles has a relationship with its micro and nano-structures. Also, it is recorded that carbon materials with regular graphite structure have lower activation energy and higher oxidation reactivity than carbon materials with a messy interior amorphous structure. For instance, Müller et al. [13] and Su et al. [14] explored the difference in PM oxidation characteristics from CI engines. It was observed that the changes in micro-structure of the particles affected the oxidation reactivity of the particles. While they found that the particles produced by different CI engines have approximately the same initial oxidation temperature. Some investigations have also been carried out to find the relationship of the particle nano-structure with soot reactivity [15–17] and it was found that the rise in fringe length or drop in tortuosity caused decrease in particle oxidation reactivity.

Since the CI engines produce a large amount of PM, thus, several studies have been carried out using different methods for reduction in PM. The alternative fuels (especially biodiesel and alcohols) in pure form, or blended form with diesel fuel, have been widely tested in the literature. The recent studies conducted in 2020 also confirm that the use of biodiesel and alcohols in CI engines [18–21] and alcohols in spark ignition engines [21–30] is still an attractive method in automotive fields. However, in CI engines, most of the former studies were conducted for exploring the influence of alternative fuels on engine combustion, performance, emissions and PM [18–21,31–42], while the majority of the investigations in regard to the PM focused on the mass, number and geometric mean diameter (GMD) of the PM. And only a few investigations have been conducted for exploring the influence of alternative fuels (only one or two types of fuels) on the structure (both micro and nano-structures), volatility and oxidation reactivity of PM from CI engines. For instance, Tse et al. [43,44] examined the soot properties on a CI engine under five different engine torques at an engine speed (1800 rpm), using several fuels including pure diesel, pure biodiesel, diesel-biodiesel (DB) and diesel-biodiesel-ethanol (DBE). According to the results, the rise in oxygen concentration of fuel caused increase in amorphous nano-structure of the PM as characterized by reduction in primary particles and agglomerates sizes. Also, they found that rise in fuel oxygen content caused decrease in fringe separation distance as well as fringe length, however, rise in tortuosity in comparison with those of PM emitted from diesel fuel. Their Thermogravimetric analyzer (TGA) results showed that the rise in oxygen concentration of fuel caused drop in soot non-volatile substances, ignition temperature, activation energy and frequency factor, but, increase in oxidization reactivity rate in comparison with those of PM emitted from diesel fuel. Zhang and Balasubramanian [45] analyzed the impacts of DB and diesel-butanol (DBu) fuels on the soot volatility and oxidation reactivity from a CI engine under various engine loads. They found that both blended fuels caused drop in soot non-volatile substances, ignition temperature and activation energy, but, rise in soot volatile organic fraction and oxidization reactivity compared to diesel fuel, while DBu had more impact than DB on these parameters.

Luo et al. [46] examined the impact of mixing acetone-butanol-ethanol (ABE, using up to 30% by volume percentage) with diesel fuel on the micro and nano-structures and oxidation reactivity of soot from a CI engine. They observed that the rise of ABE content in diesel fuel resulted in drop in average diameter and fringe length of primary particle, but, increase in tortuosity and oxidization reactivity of particle, while the soot nano-structures become more

amorphous in nature. Zhu et al. [47] examined the influence of diesel, biodiesel and biodiesel-pentanol (BP) fuels on the soot micro-structure, volatility and oxidization reactivity on a CI engine. According to their results, the increase in pentanol concentration in the BP blend caused decrease in primary particle size. TGA results showed that both biodiesel and BP fuels led to drop in particle non-volatile substances compared to those parameters of diesel fuel, while the biodiesel had higher reduction effect than BP. Also, they found that the particle semi-volatile fraction and oxidization reactivity increase is in the order of diesel < BP30 < BP20 < BP10 < biodiesel.

Fayad et al. [48] conducted several tests to analyze the PM morphology and micro-structure of a CI engine equipped with a diesel oxidation catalyst fueled with diesel, biodiesel and diesel-biodiesel-butanol (DBBu). According to the results, both biodiesel and DBBu caused reduction in primary particle and agglomerates sizes and decrease in primary particles number and fractal dimension compared to those of diesel fuel. In another work, Fayad et al. [49] also found that the DBu had lower primary particles number, primary particle size, radius of gyration and fractal dimensions than those of diesel fuel. Ghadikolaei et al. [50] reported that DBE fuel reduced primary particle size and fringe length, but, increased fringe separation distance and had no effect on fringe tortuosity compared to those of diesel fuel in a 4-cylinder CI engine under several engine speeds and loads conditions.

The literature, as mentioned above, shows that various studies have been carried out to understand the impacts of alternative fuels (especially biodiesel and alcohols) on the engine combustion, performance and gaseous emissions. However, in regard to PM emissions, only PM mass, number and GMD have been comprehensively investigated, while there are still: a) lack of knowledge about the micro and nano-structures, volatility and oxidation reactivity of diesel PM; also b) no available comprehensive study to understand the influence of various alternative fuels, including biodiesel, methanol, ethanol, butanol and pentanol, on the micro and nano-structures, volatility and oxidation reactivity of PM, in the literature. Therefore, this experimental research is presented to tackle these two knowledge lacks. The PM samples for this study are taken from a CI engine for low and high loads at 1800 rpm on dynamometer tests to explore the impacts of diesel, pure biodiesel (waste cooking oil as feedstock) and different ternary alcohol blends (diesel-biodiesel-alcohol) on the structure (both micro and nano-structures), volatility and oxidation reactivity of diesel PM, and also to investigate the relationship between these parameters. Four alcohols including methanol, ethanol, butanol and pentanol, were blended separately with diesel and biodiesel to form four ternary fuels. The overall oxygen concentration of each ternary blended fuel was fixed at 6% by mass for establishing the same condition for comparing. In order to ensure that biodiesel contributed the same oxygen concentration to the blended fuels and the final mixed fuel had a good miscibility (too high content of alcohol fuel can cause fuel incompatibility, especially for methanol), the percentage of biodiesel in all blended fuels was fixed at 33% by mass.

2. Experimental setup and procedure

2.1. Test procedures and fuel properties

The experiments for this research were carried out on a 4-cylinder, direct injection CI engine, and the basic parameters of the CI engine are shown in Table 1. The CI engine was connected to an eddy current dynamometer, and the Ono Sokki engine controller system was utilized to adjust the speed and the torque of the CI engine. The Ono Sokki engine controller automatically adjusts the rate of each fuel based on its energy content (calorific value) to maintain the desired engine power (speed and torque) constant. The experimental system for the present work is shown in Fig. 1. The experiments were conducted under a fixed engine speed of 1800 rpm at low (10%) and high (80%) engine loads. The brake mean effective pressure (BMEP) levels corresponding to 10% and 80% maximum engine torque were 0.08 MPa and 0.66 MPa,

Table 1
Basic parameters of the CI engine.

Engine model	ISUZU 4HF1
Type	In-line 4-cylinder
Maximum power	88kW/3200 rpm
Maximum torque	285Nm/1800 rpm
Bore/stroke	112mm/110 mm
Displacement	4.334L
Compression ratio	19.0:1
Fuel injection timing (BTDC)	8°
Injection pump type	Bosch in-line type
Injection nozzle	Hole type (with 5 orifices)

respectively.

Six fuels including Euro V diesel (D100), biodiesel (B100) with waste cooking oil feedstock, diesel-biodiesel-methanol (DBM), diesel-biodiesel-ethanol (DBE), diesel-biodiesel-butanol (DBBu) and diesel-biodiesel-pentanol (DBP) were tested. All the alcohols utilized had high purities of over 99.8%. The blending principles of the alcohol blends are as follows: Firstly, the mass fraction of biodiesel is guaranteed to be 33%, and then the mass percentages of the other two blended fuels are respectively calculated to achieve the same oxygen concentration of 6% by mass. The reason for fixing the proportion of biodiesel at 33% by mass is to ensure that the concentration of each alcohol fuel in the corresponding ternary fuel can be maintained at an appropriate level when the oxygen concentration of each ternary fuel is fixed at 6% by mass. If the proportion of biodiesel is too low, the proportion of alcohol fuel will be correspondingly higher. Higher proportion of alcohol fuels will eventually lead to the incompatibility of some of the blended fuels, like DBM and DBE. On the other hand, higher proportion of biodiesel will lead to an excessively low proportion of alcohol fuels, which cannot show the impact of alcohol fuels on the final results. Table 2 shows the fuel mixing ratio and composition, and Table 3 gives the properties of the base fuels and different ternary blends. All the alcohol blended fuels were stored for two weeks and no separation was observed. The experimental errors involved in this study were calculated according to Ref. [51]. Student's t-test was also employed to verify the differences between experimental results obtained from various fuels and

conditions have statistically significant at a confidence level of 95%.

2.2. PM sampling and analysis

2.2.1. Micro and nano-structures of PM

The particle micro and nano-structures parameters in this study were obtained by a Field emission-scanning transmission electron microscope (STEM, Jeol JEM-2100F) with a maximum magnification of 910k times and a corresponding resolution of 0.2 nm. Magnifications of 20k, 80k and 400k (corresponding to the resolutions to obtain the images in 200 nm, 50 nm and 20 nm, respectively) were chosen for observing the micro and nano-structures of the particles.

To collect the samples, direct and in-direct particle sampling methods are available according to the literature for study the micro and nano-structures of particles emitted from engines. For the direct particle sampling method, the TEM grid is directly located in front of particle origin with the use of collectors like probes which can be operated according to the thermophoresis, aerodynamic quenching or N₂ dilution [55–61]. In this method, the collector can be placed in various locations to obtain the particle samples, including inside the engine cylinder (as in-flame particle sampling method) [62–66], in the engine exhaust line [63,65,66] or after a dilution system [67,68]. But, in-flame sampling suffers some drawbacks. For example, it is difficult and needs more efforts to insert the collector inside the engine cylinder. In addition, the

Table 2
Fuel mixing ratio and composition.

Based fuels	Diesel	Biodiesel	Methanol	Ethanol	Butanol	Pentanol
D100	100%					
DBM	62.13%	33%	4.87%			
DBE	60%	33%		7%		
DBBu	55.72%	33%				11.28%
DBP	53.56%	33%				
B100			100%			13.44%

*The oxygen concentrations of all alcohol blends are ensured to be 6% by mass.

*All fuel ratios are based on the mass percentage.

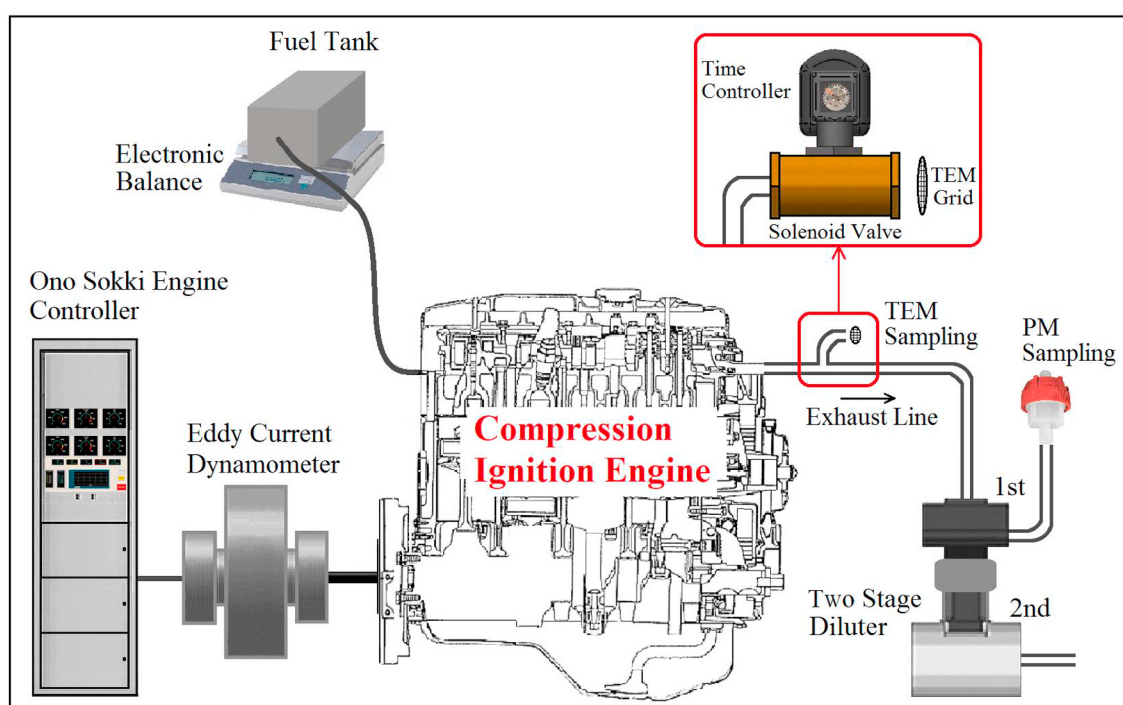


Fig. 1. Experimental system.

Table 3
Properties of base fuels and different ternary blends.

Properties	Cetane number	Lower heating value (MJ/kg)	Density (kg/m ³) at 20 °C	Viscosity (mPa S) at 40 °C	Heat of evaporation (kJ/kg)	Boiling point (°C)	Flash point (°C)	Carbon content (% mass)	Hydrogen content (% mass)	Oxygen content (% mass)
Diesel [52] ^a	52.0	42.50	840.0	2.40	270.0	180–360	78.0	86.60	13.40	0
Biodiesel [52] ^a	51.0	37.50	871.0	4.60	300.0	—	210.0	77.10	12.10	10.80
Methanol [53] ^a	5.0	19.58	791.3	0.58	1162.6	64.7	12.0	37.48	12.58	50.00
Ethanol [52] ^a	8.0	26.83	789.4	1.13	918.4	78.3	17.0	52.14	13.00	34.80
Butanol [54]	17.0	33.09	809.7 ^b	2.22	581.4	117.5	35.0	64.82	13.60	21.60
Pentanol [54]	18.2	34.65	814.8 ^b	2.89	308.1	137.9	49.0	68.13	13.72	18.15
DBM								81.07	12.93	6.00
DBE								81.05	12.94	6.00
DBBu								81.01	12.99	6.00
DBP								80.98	13.01	6.00

^a From the same laboratory.

^b At 15 °C.

primary particles and aggregates might not be completely produced into their original shapes because of the short period time from the combustion and particle sampling. Similar to the in-flame particle sampling method, TEM sampling after diluter also has some disadvantages. For instance, a long sampling line and time from the engine to the end of diluter, and the use of diluent (air) have influences on the particle structures.

On the other hands, for in-direct particle sampling, the existing method for collecting particles is to collect the PM by a filter (mostly 47 mm quartz filter) from the engine exhaust (before or after diluter), and then extract the particles from the filter by solvents (like ethanol and methanol). Next, some droplets of the particles accompanying with solvent are dropped on a TEM grid. Finally, after drying the TEM grid, the sample is ready for micro and nano-structures analysis [69–73]. However, this PM sampling method has some disadvantages which affect the particle physicochemical properties due to using liquid medium [74,75] and also original configuration morphology of the PM cannot be observed.

For this research, for preventing the drawbacks of in-flame, after dilution or filter particle sampling methods as discussed before, the particle sample for the micro and nano-structures analysis was directly obtained from the engine exhaust line on a TEM grid with the use of a solenoid valve alongside with a time controller [50] as shown in Fig. 1. The time controller used in this study had an operating time accuracy of ±1%. The hot particles emitted from the engine exhaust pipe were stuck on the TEM grid as a consequence of thermophoretic impact [66]. The TEM grid used was a 3 mm copper grid consisted of 400 meshes which was covered by holey-carbon film. The sampling time according to the operating conditions were 1 s for low engine load (BMEP = 0.08 MPa) and 100 ms for high engine load (BMEP = 0.66 MPa). These sampling times were chosen after taking several pretests using STEM to get the suitable sampling times to obtain sufficient particles and aggregates deposited on the TEM grid.

In this research, the particle micro-structure parameters including primary particle diameter and its distribution, and the particle nano-structure parameters including fringe length (L_a), tortuosity (T_f) and fringe separation distance (D_s) were obtained via an image analyzing software (Image-Pro Plus 6.0; Media Cybernetics). The method for obtaining the primary particle diameter and distribution is as follows. Firstly, in image analyzing software, several particles with clear boundaries are manually selected by the operator from the low-resolution images, and the software can automatically calculate the size of each particle. Then, the distribution of the primary particles can be obtained. The nano-structure parameters are obtained by analyzing

the high-resolution images through the following steps. Firstly, the TEM image is converted into a frequency-domain signal by Fourier transform, then the Gaussian filtering method is used to remove the interference signal in the frequency domain signal, and then the electron microscope image is re-obtained by the inverse Fourier transform, and finally recovered by the binary method. At this time, the image is changed from a gray-scale structure with a blurred carbon layer structure to a black-and-white image with a clear carbon layer. Then the carbon layer is changed into a carbon frame line by image skeletalization, and then the carbon frame line parameters are manually selected. The detailed processing method is described in Refs. [76].

Since L_a , T_f and D_s have a relationship with PM physico-chemical properties [77], thus, they were chosen for nano-structure analysis in this work. As shown in Fig. 2, L_a shows the physical extent of the atomic carbon layer planes, in unit of nanometer (nm). T_f is a non-dimensional ratio of fringe length to the distance between the two endpoints. And D_s illustrates the mean distance between the adjacent carbon layer planes, in unit of nm [76]. In regard to reducing the results error, for obtaining the primary particle diameter and its distribution, 100 particles with clear boundaries from 10 to 15 TEM images, were selected. For the statistics of the nano-structure parameters of the particles, 30 regions of interest (ROI) from the high-resolution images, were selected. The averages of these observations are presented in this study.

2.2.2. Volatility and oxidation reactivity of PM

The thermogravimetric analysis was applied to explore the particles volatility and oxidation reactivity. The thermogravimetric loss curve of the particle sample was examined by a Thermogravimetric analyzer/Differential scanning calorimeter (TGA/DSC3+, Mettler Toledo) to analyze the oxidation reactivity of the particles. In general, particles emitted from engines have two significant mass loss stages in the range of ambient temperature up to 850 °C. The first stage is de-volatilization stage for those volatile components in the particles which can be completely volatilized in an inert gas (such as argon, helium, nitrogen or etc.) in the temperature less than 400 °C. The second stage is for non-volatile soot components that would be fully oxidized in an air atmosphere above 400 °C until 850 °C (oxidation stage). Therefore, particles emitted from engines can be divided into two parts, volatile parts and non-volatile parts. The particle samples used in the thermogravimetric analysis were obtained from the 100% pure quartz fibre filter (type QM-H, Whatman™, Sweden) which could be heated up to 900 °C. PM samples were taken from the first-stage diluter (as shown in Fig. 1) with a dilution ratio of about 6. Part of quartz fibre filter containing PM was put into an Alumina crucible and then placed into the TGA/DSC

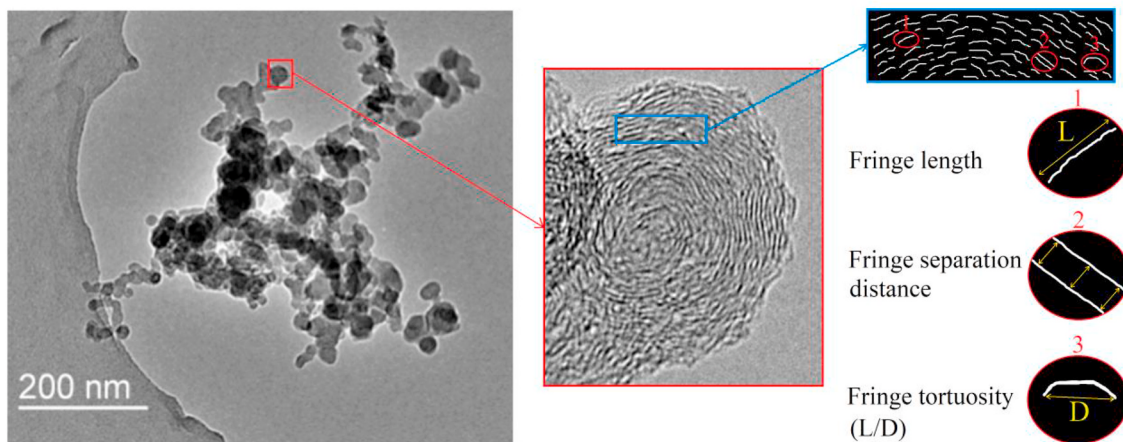


Fig. 2. Schematic of particle nano-structure parameters.

equipment for analysis. The two-stage heating program adapted for this study, is presented in [Table 4](#).

3. Results and discussion

3.1. Particle micro-structure

Different working conditions of the CI engine will affect the morphology of the particles. In this section, the TEM grid loaded with particles was amplified by 20k times through the high magnification electron microscope to observe the microscopic topography of the particles produced by various fuels under both low and high engine loads.

3.1.1. Morphology of aggregate particles

[Figs. 3 and 4](#) show the microscopic topography of the aggregate particles produced by the CI engine fueled with D100, DBM, DBE, DBBu, DBP and B100 at the low engine load ($BMEP = 0.08 \text{ MPa}$) and high engine load ($BMEP = 0.66 \text{ MPa}$), respectively. It can be clearly seen from [Figs. 3 and 4](#) that as the engine load increases, the number of primary particles increases which causes increase in size of the aggregate particles. The reason for this phenomenon is that due to the rise of engine load, more fuel is injected into the combustion chamber to burn, resulting in the generation of more primary particles and increases in collision rate between the primary particles and hence increases in size of the aggregate particles.

As can be seen from [Figs. 3 and 4](#), the aggregate particles consist of dozens or hundreds of spherical or quasi-spherical primary particles, which are gathered in a cluster or chain shape for all the tested fuels, while the number of primary particles and size of the aggregate particles produced by D100 are significantly higher than those of other fuels. By comparing the PM formed by B100 and the alcohol blended fuels with that produced by D100, it can be found that the particle agglomerates and clusters from B100 and the alcohol blends contain smaller primary

particles and fewer number of primary particles. This can be attributed to the biodiesel and alcohols properties. For instance, the lower cetane number of the alcohols makes the diffusion combustion phase shorter (due to longer ignition delay), and the higher oxygen content of biodiesel and the alcohols can make the oxidation reactivity faster [36,43, 79], thus, both of them reduce the number and size of the primary particles. In addition, no aromatic components, lower carbon content and higher oxygen content of biodiesel and the alcohols cause reduction in the nuclei particles formation, resulting in the formation of smaller primary particles than diesel fuel [43]. Comparing with the different ternary fuels, it can be observed that the ethanol blend has the lowest number of primary particles in the particle agglomerates and clusters. Smaller primary particle diameter and particle agglomerates size with the application of oxygenated fuels compared to those of diesel fuel were also recorded in the literature [43,70,73,80,81].

3.1.2. Primary particle size distribution

[Figs. 5 and 6](#) illustrate the primary particle size distribution obtained by a random selection of about 100 primary particles from 10 to 15 TEM images for different fuels under low and high engine loads, respectively. From [Figs. 5 and 6](#), it can be clearly seen that with the rise in engine load, the primary particle size distribution gradually increases towards larger sizes for all the tested fuels. This is mainly due to the fact that as the load increases, the air-fuel ratio of the CI engine decreases, and the inhomogeneity of the fuel-gas mixture in the cylinder increases. These are favorable for the formation of larger primary particles. Also, large-size particle agglomerates are generally formed at the later stage of combustion. For high load, the combustion duration (diffusion mode) increases, and the time for particles to grow in the cylinder is more sufficient, so the primary particle size is bigger.

According to [Fig. 5](#), the primary particles produced by all the tested fuels are basically distributed in the range of 10–40 nm, and the peak value is between 15 and 30 nm. While the size of primary particles produced by the combustion of diesel fuel is larger than that of other fuels and the particles are mainly (proportion of 60%) located in the range of 20–27.5 nm. The particle size of alcohol blended fuels is basically distributed in the range of 20–25 nm, while DBM had the smallest value. While the primary particles produced by biodiesel have the smallest size among all the tested fuels, with more than 70% of them in the range of 15–25 nm.

[Fig. 6](#) shows the primary particle size distribution of different fuels under high load condition. For diesel fuel, the particle size is mainly distributed in the range of 25–30 nm, which is 2–3 nm higher than that under the low load. The diameter of biodiesel generated particles is mainly distributed in the range of 17.5–27.5 nm (proportion of 70%). The primary particles size of the alcohol blended fuels is in the range of

Table 4
Thermogravimetric temperature control program [78].

Stage	Program
I	De-volatilization
Step 1	Initial gas atmosphere: nitrogen
Step 2	Isothermally set for 10 min
Step 3	Heating up to 45 °C at a rate of 3 °C/min
Step 4	Heating up to 400 °C at a rate of 10 °C/min
II	Oxidation
Step 5	Change the atmosphere to air
Step 6	Heating up to 850 °C at a rate of 10 °C/min
Step 7	Isothermal for 10 min
Step 8	Cooling to room temperature

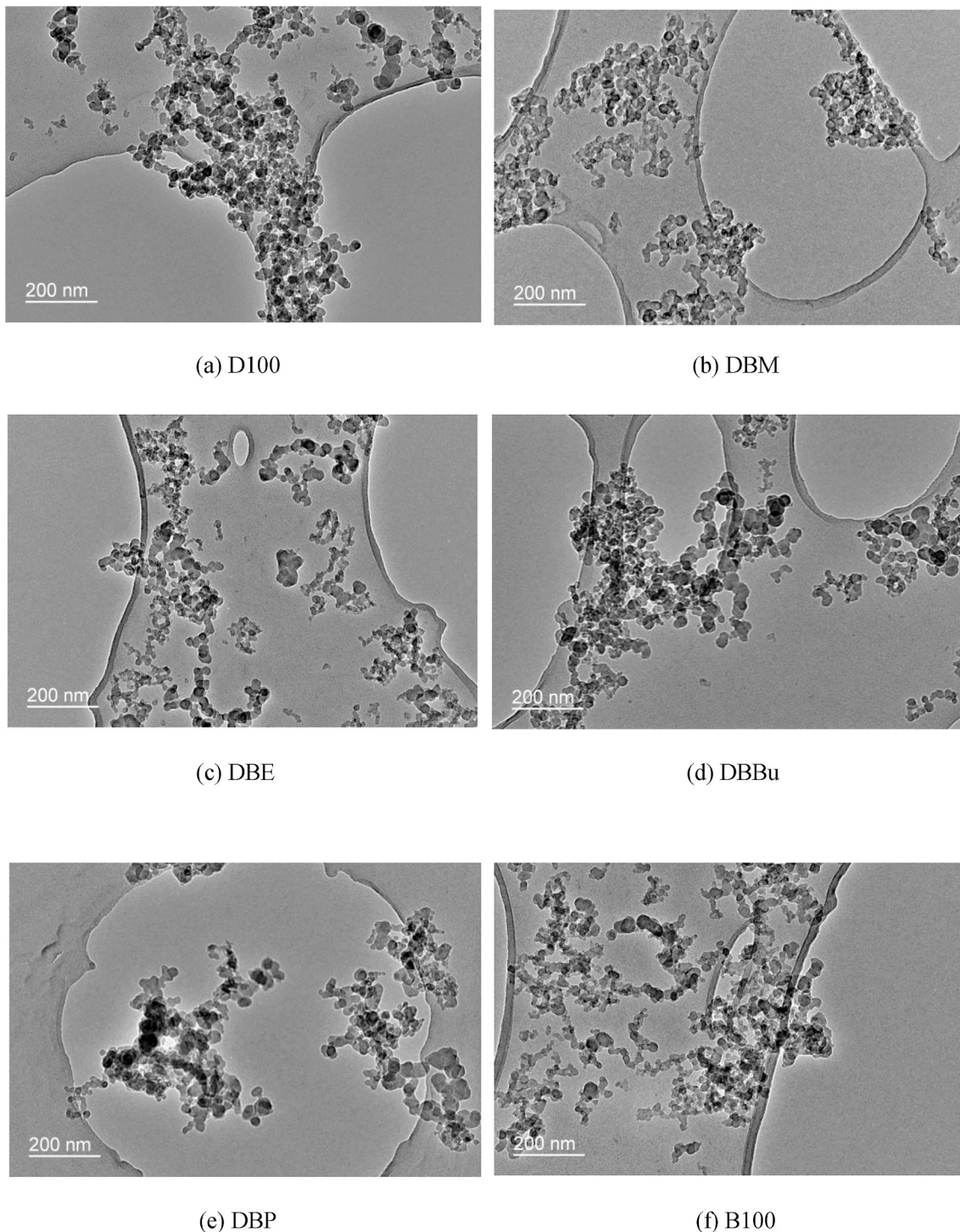


Fig. 3. Medium magnification STEM images of PM for various fuels under low engine load.

20–30 nm, while DBM has the smallest value (between 20 and 27.5 nm) among the tested alcohol blends. As mentioned above (in the morphology of aggregate particles section), biodiesel and the alcohols contain no aromatic components, which reduces the growth of primary particles, while the oxygen atoms contained in the biodiesel and alcohol fuels contribute to the oxidation of the primary particles, thereby reducing the primary particles size.

The finding in the present study can be supported by the former study using scanning mobility particle sizer (SMPS) [82]. Because, among the tested ternary fuels, DBE in this research has the lowest number of primary particles in the particle agglomerates and clusters

which is the same as finding the lowest total particle number concentration achieved by DBE [82], and the lowest primary particle diameter in this study is recorded for DBM which is the same as the finding of the smallest geometric mean diameter achieved by DBM [82].

3.2. Particle nano-structure

Different working conditions of the CI engine will affect the particle nano-structure. In this section, the TEM grid loaded with particles was amplified by 400k times through STEM to observe the nano-structure of the particles produced by various fuels under both low and high loads.

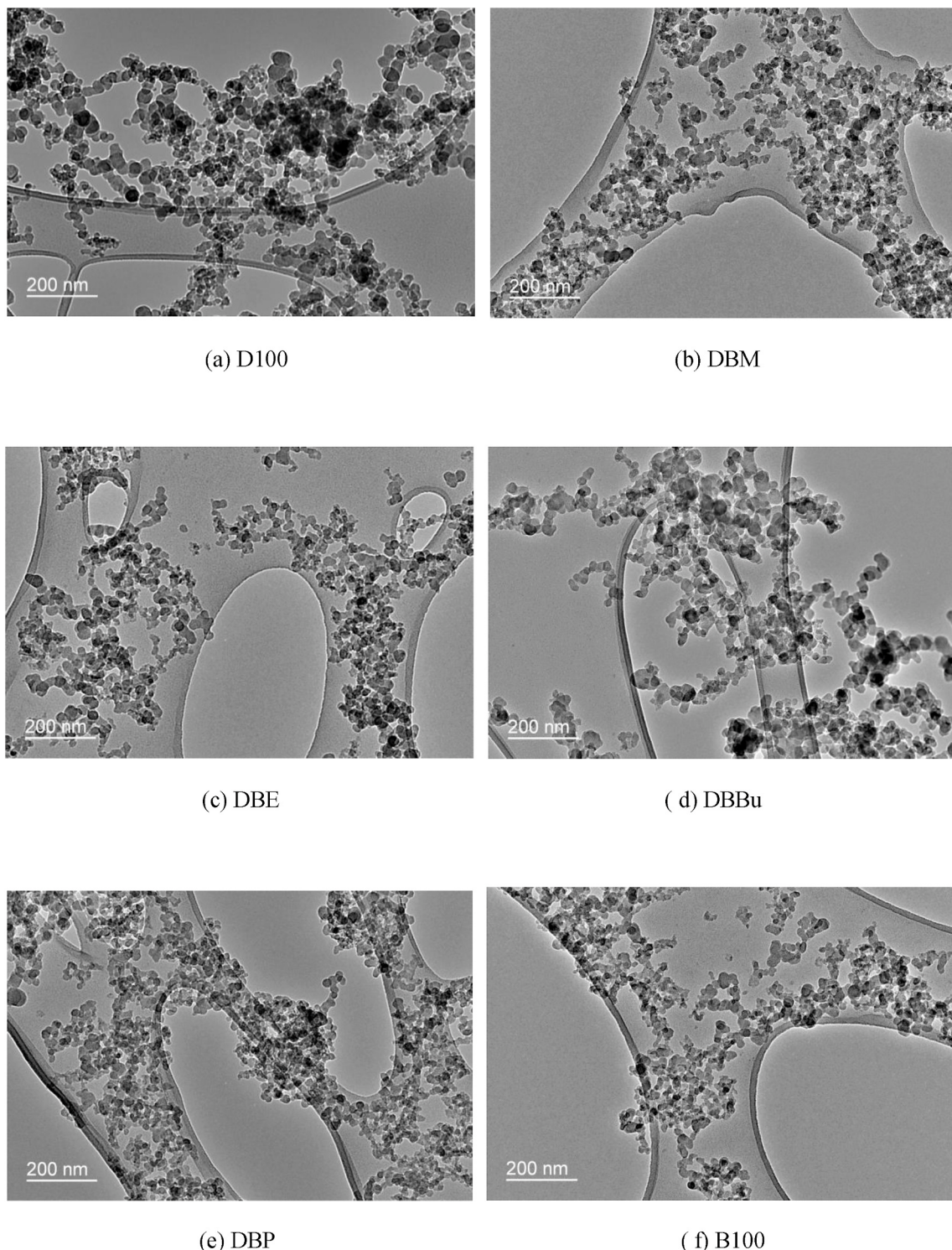


Fig. 4. Medium magnification STEM images of PM for various fuels under high engine load.

3.2.1. Morphology of primary particle

Fig. 7(a–f) reveals the STEM images of the nano-structure of the primary particles produced by different fuels under low load condition. According to **Fig. 7(a–f)**, the primary particles have a nearly circular carbon layer structure. The near-circular carbon layer structure shows a two-dimensional structure of the core-shell, in which the core shows the curved and irregularly arranged carbon structure, and the shell is generally a microcrystalline carbon layer structure with different levels of wrinkles. **Fig. 7(g–l)** shows the STEM images of the nano-structure of

the primary particles produced by different fuels under high load condition. According to **Fig. 7(g–l)**, the primary particles have a pronounced shell-core structure under high load condition. The inner core usually exhibits a nearly round, regular carbon crystal structure, and the shell is generally clear and neatly arranged with no obvious fold. In addition, primary particles can also be categorized into non-core particles, single-core particles and multi-core particles. Non-core particles generally indicate that no clear-shaped core structure can be found in the primary particle center, which can be seen from primary particles produced by

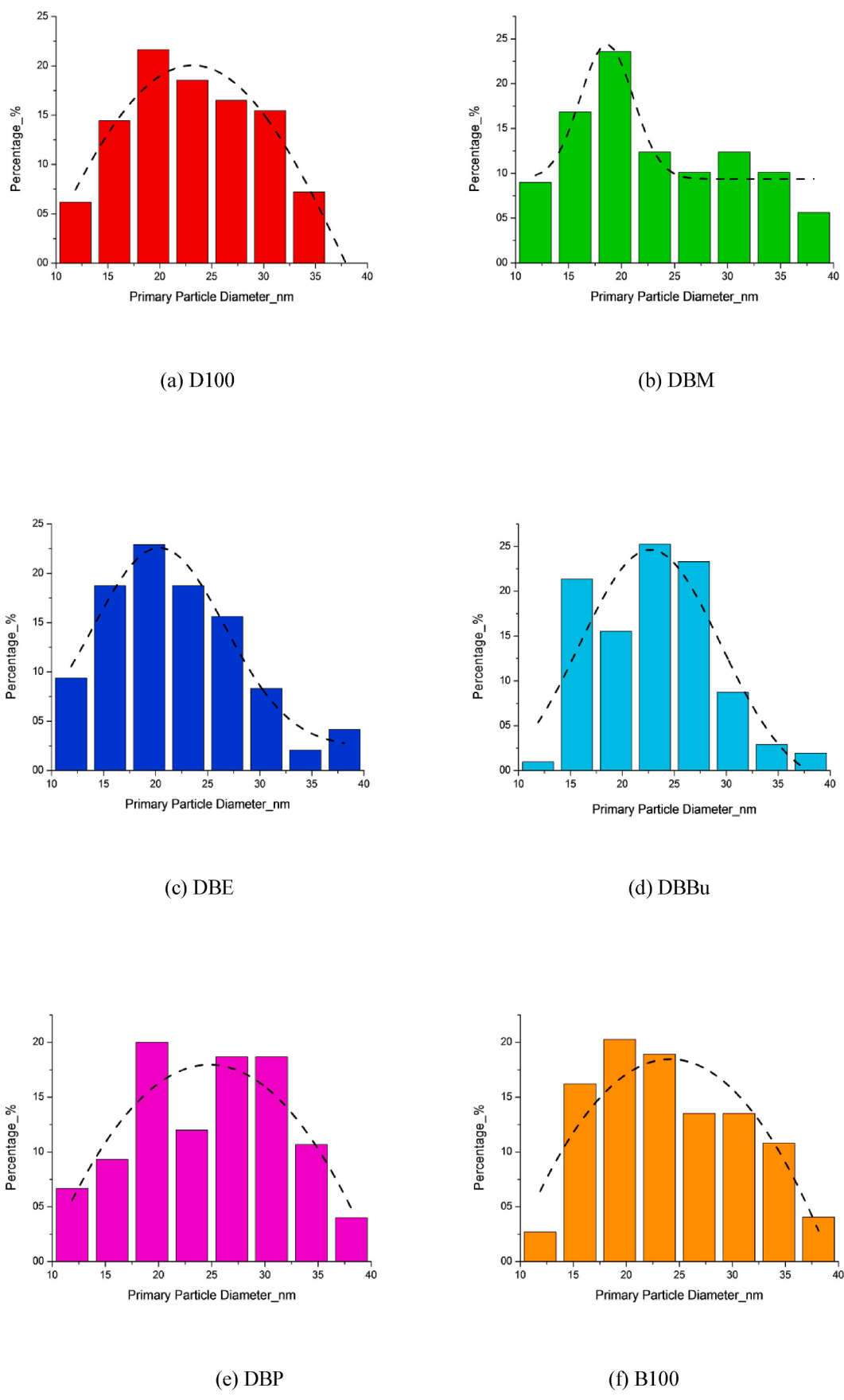


Fig. 5. Primary particle size distribution for various fuels at low engine load.

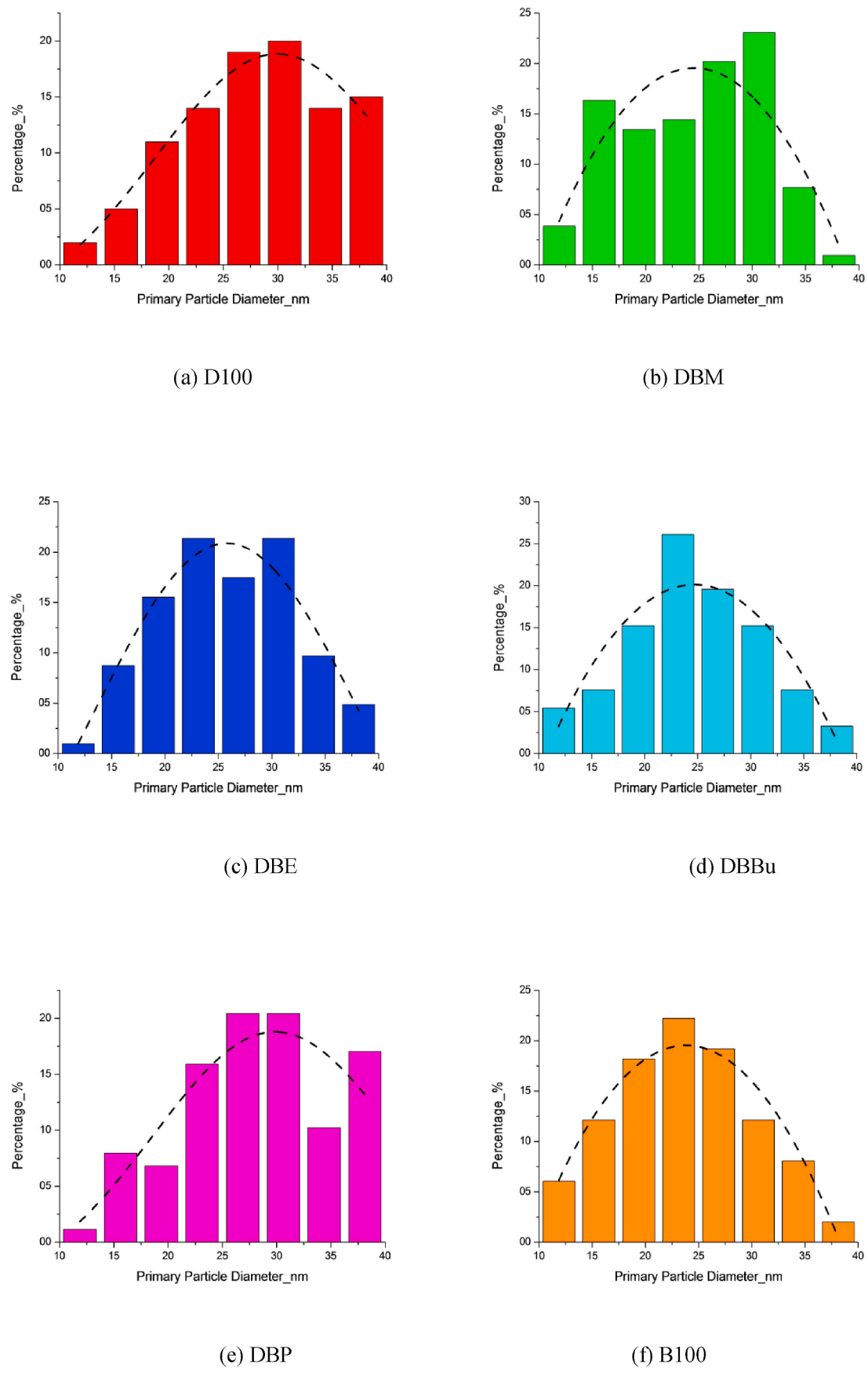


Fig. 6. Primary particle size distribution for various fuels at high engine load.

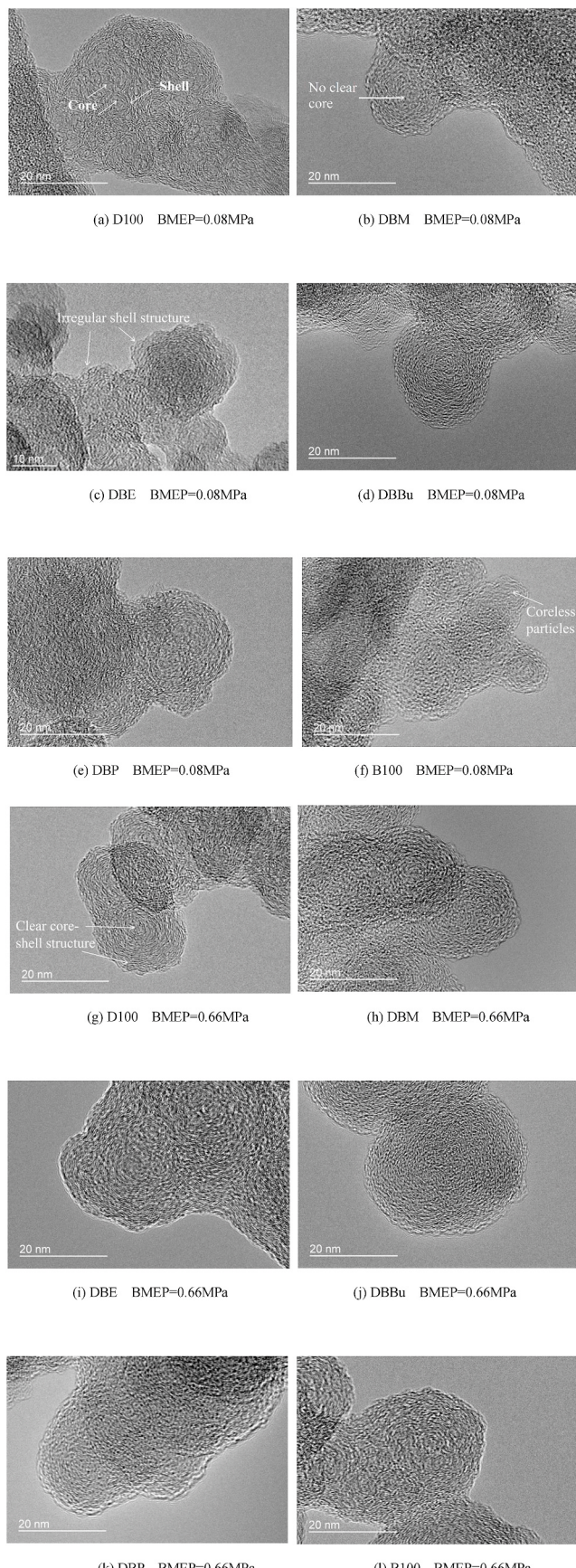


Fig. 7. High magnification STEM images of PM for various fuels under low (a–f) and high (g–l) engine loads.

biodiesel under low load condition (Fig. 7 (f)). Single-core carbon particles illustrate the presence of an amorphous carbon structure in the central region of the primary particles produced by alcohol blended fuels (Fig. 7(b–e)). Multi-core particles generally have a plurality of amorphous carbon structures in the central region in the primary particles with a size range of 30–40 nm, which are generally exhibited in common diesel fuel generated particles (Fig. 7 (a)). This can also confirm the results above, that the primary particle diameter from diesel fuel is generally larger than that of other fuels (e.g. biodiesel and alcohol blends). Primary particles of alcohol blended fuels, especially DBM and DBE, have carbon layer morphologies similar to those of biodiesel, and also exhibit an irregular “core-shell” structure with no clear core. Since methanol and ethanol have shorter chains in their structures than other alcohols, therefore, their hydroxyl radical ($\cdot\text{OH}$) and oxygen can be extracted easier from their molecule decomposition during combustion, causing in increasing the oxidizing ability of the particles, having more volatile substances [36] and hence changing the PM nano-structure (irregular PM structure compared to PM from diesel fuel) due to changes in fringe length and tortuosity. In addition, viscosity of the blends containing methanol and ethanol is almost close to each other and lower than other alcohols blends, resulting in better fuel atomization and hence decrease in the primary particles number and size (Figs. 3–6), total number concentration, GMD and PM mass [82], therefore, $\cdot\text{OH}$ and oxygen have more access to change the PM nano-structure by reducing the fringe length and forming of curved carbon layers (higher tortuosity) compared to other alcohols. The observation is consistent with the results above for the primary particles size for biodiesel, DBM and DBE. Because, the irregular “core-shell” structure of primary particles for biodiesel, DBM and DBE causes weaker connection of the outer carbon layers and increase in oxidation reactivity of the primary particles, resulting in decrease in primary particle size.

3.2.2. Particle nano-structure parameters

Table 5 shows the nano-structure parameters (including L_a , T_f and D_s) of primary particles produced by the CI engine with various fuels under both low and high load conditions. As can be seen from Table 5, for all the tested fuels, as the load increases, the average L_a of the particles gradually increases, while T_f and D_s decrease which are in line with the results of other investigations [10,17,73,80,81]. Under low load condition, L_a corresponding to the diesel fuel is the largest, ranging from 0.768 to 0.817 nm. L_a produced by biodiesel is lower than that parameter for diesel fuel, and it is decreased by 17.1–27.3%. For alcohol blended fuels, L_a is located between those of diesel fuel and biodiesel. The DBM achieves the lowest L_a among the tested alcohol blends, and it is between 0.599 and 0.667 nm which is 13.2–26.7% lower than that of diesel fuel. Under high engine load, L_a from diesel fuel is between 0.833 and 0.891 nm, which is approximately 10% higher than that for the low engine load condition. For the alcohol blended fuels, minimum L_a is recorded for DBM, and it is between 0.667 and 0.686 nm, which is

Table 5
Particle nano-structure parameters for various fuels under low and high engine loads.

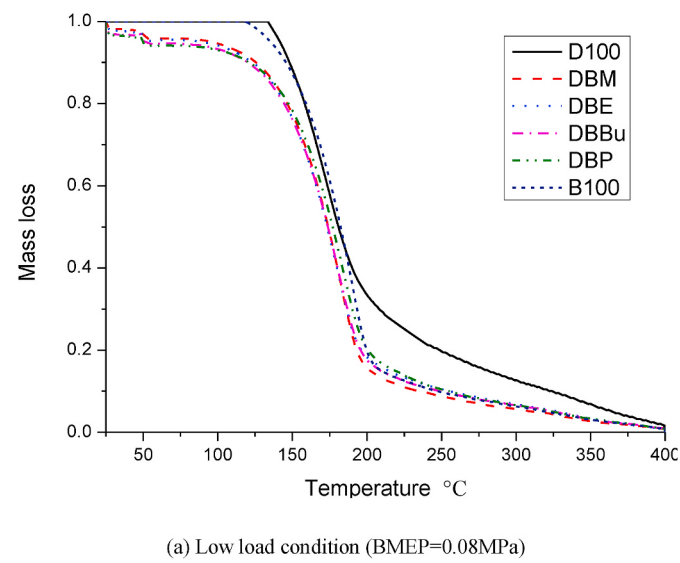
Fuel	Load(MPa)	$L_a(\text{sd})/\text{nm}$	$T_f(\text{sd})$	$D_s(\text{sd})/\text{nm}$
D100	0.08	0.793(0.0246)	1.124(0.0729)	0.352(0.0412)
	0.66	0.857(0.0245)	1.102(0.0767)	0.324(0.0408)
DBM	0.08	0.633(0.0332)	1.264(0.1541)	0.363(0.0436)
	0.66	0.657(0.0337)	1.248(0.1558)	0.345(0.0347)
DBE	0.08	0.676(0.0107)	1.246(0.1648)	0.369(0.0419)
	0.66	0.702(0.0114)	1.238(0.1654)	0.338(0.0319)
DBBu	0.08	0.712(0.0426)	1.263(0.1148)	0.357(0.0395)
	0.66	0.735(0.0435)	1.246(0.1123)	0.349(0.0287)
DBP	0.08	0.714(0.0389)	1.274(0.2013)	0.354(0.0325)
	0.66	0.721(0.0391)	1.269(0.2019)	0.329(0.0356)
B100	0.08	0.617(0.0203)	1.316(0.1505)	0.371(0.0425)
	0.66	0.658(0.0253)	1.287(0.1567)	0.343(0.0414)

12.7% higher than that for the low engine load.

T_f for the particles from the CI engine for various fuels for both low and high engine loads is shown in Table 5. Diesel fuel has the lowest T_f at both low and high loads, which is between 1.052–1.196 nm and 1.026–1.179 nm, respectively. The difference in T_f between the two loads is less than 2% (insignificant difference with T-test). Among the tested alcohol blends, DBM shows the highest T_f , and it is located between 1.093–1.423 nm and 1.101–1.429 nm at low and high load conditions, respectively. D_s of the primary particles produced by all six fuels is basically within the range of 0.324–0.371 nm under both loads. It can be found that D_s of the carbon layers of the primary particles is not significantly affected by the fuel physicochemical properties and the engine load. According to Table 5, the application of biodiesel and alcohol fuels decreases L_a (22.7% for biodiesel and about 16% for the alcohols in average) and increases T_f (16.9% for biodiesel and about 13% for the alcohols in average) and almost has no effect on D_s (5.6% increase for biodiesel and about 4% increase for the alcohols in average, but, the differences are not significant with T-test) in comparison with those of PM from diesel fuel. In general, longer L_a , and lower T_f and D_s of primary particles show poor oxidative reactivity of particles (as described in the next section).

3.3. Particle volatility and oxidation reactivity

The particle mass reduction curve shows the variation of mass loss with temperature, which can reflect the volatility and oxidation characteristics of the PM. The volatility of particle in this study refers to 1) volatile substances (mostly OC) which can be measured from the TGA furnace temperature range of 50–400 °C in a nitrogen atmosphere, and 2) non-volatile substances (mostly EC) which can be measured from the TGA furnace temperature range of 400–850 °C in an air atmosphere [79]. Fig. 8 shows the particle mass reduction curves from 25 °C (ambient temperature) to 400 °C for different fuels under low (a) and high (b) engine loads. From Fig. 8, it can be seen that the mass loss rate from all the tested fuels under low engine load is higher than that of the high engine load, which indicates that the particles produced under low load condition have higher volatility due to more organic carbon (OC) and less elemental carbon (EC) in the PM at low engine load. It can be found that the mass loss rate of PM produced by biodiesel and the alcohol blended fuels is faster than that of diesel at both engine loads which shows that biodiesel and the alcohol blended fuels have higher PM volatility than diesel under the same working conditions. For the alcohol blends, there is no significant difference in the mass loss starting temperature and mass loss rate among them under the low load condition, but the mass loss rate of PM from DBM is significantly higher than that from the other blended fuels under high load condition. This also shows that the particles produced from DBM have the highest PM volatility. Since methanol has the simplest alcohol structure, therefore, its shorter chains cause easy extraction of •OH and oxygen from their molecule decomposition during combustion, causing in increasing the oxidizing ability of the particles and having more volatile substances compared to other alcohols with longer chains [36]. Also, the active carbon on the C–H bond at the edge of the ternary fuels, especially methanol has a stronger impact than the other alcohols. As a result, these carbon atoms at the edge are more likely to chemical reaction with the surrounding •OH and oxygen, thereby increasing the oxidizing ability of the particles. In addition, the methanol blend has a short diffusion combustion phase period [82], which limits the agglomeration and coalescence of the late combustion particles, ultimately resulting in achieving the lowest primary particle size and fringe length, and the highest tortuosity and PM oxidation reactivity rate as well as the highest volatile substances among all the tested fuels. Since biodiesel and the alcohol blended fuels have lower sulfur and aromatic components and C/H mass ratio, and higher oxygen content, therefore, they produce lower PM and hence lower EC, resulting in achieving higher PM volatility than diesel fuel (because diesel fuel has sulfur and aromatic



(a) Low load condition (BMEP=0.08MPa)

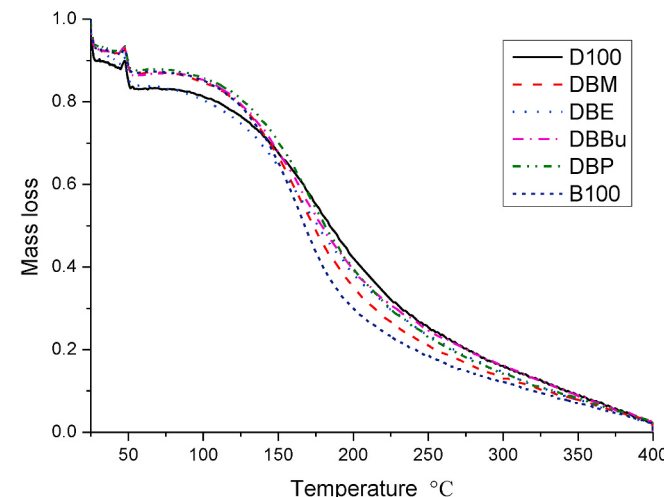


Fig. 8. Particle mass reduction curve of various fuels under low and high engine loads at 25–400 °C.

components [83,84]). Other studies also found that oxygenated fuels like DBE and biodiesel caused increase in PM volatility compared to diesel fuel [43,44,80,81,85].

It can be observed from Fig. 8 (a) that the PM from pure biodiesel has almost similar mass reduction up to about 200 °C to that of diesel fuel at low engine load. It is well known that most of the PM concentration at low engine load is made by volatile substances including unburned fuel and hydrocarbons due to incomplete combustion [79,81]. Since the combustion temperature under the low engine load condition, is very low, and biodiesel has high fuel viscosity (Table 3), therefore, its low fuel atomization rate coupled with low combustion temperature cause the formation of unburned fuels. In addition, biodiesel has the lowest brake thermal efficiency and the highest brake specific fuel consumption among all the tested fuels at low engine load of 0.08 MPa [82]. So, when the PM sample from biodiesel contains unburned fuel with larger size (compared with diesel and alcohol blended fuels) and since the flash point of biodiesel is also high (about 210 °C, Table 3), therefore, the PM from biodiesel has almost similar mass reduction up to about 200 °C to that of diesel fuel under low engine load. Wei et al. [81], also observed that the mass reduction of PM from pure waste cooking biodiesel had almost similar trend up to about 200 °C to that of diesel fuel under low

engine load, and the difference between the PM mass reduction of these two fuels was started after about 200 °C, which supports the present findings. However, at high engine load (Fig. 8 (b)), this phenomenon cannot be seen for PM from biodiesel, because the combustion temperature is very high and these fuel properties of biodiesel have almost no effect for the PM mass reduction up to about 200 °C.

Fig. 9 shows the particle mass reduction curves at 400–850 °C for various fuels under low (a) and high (b) engine loads. According to Fig. 9, the particle mass loss rate of all fuels under higher engine load condition is lower than that under low load condition due to more non-volatile substances and EC in the PM at the high engine load, and the lower air/fuel ratio under high engine load suppress the EC oxidation [86]. According to Fig. 9, the non-volatile substances mass loss rate of biodiesel and the alcohol blends is obviously higher than that of diesel fuel under both low and high engine loads, which indicates that the PM of biodiesel and the alcohol blended fuels have higher oxidation reactivity rate than that of diesel fuel. Other investigations also found that DBE and biodiesel caused decrease in non-volatile PM and increase in particle oxidation reactivity rate compared to diesel fuel [43,44,80,81, 85]. It can be seen that there is no obvious difference between the mass loss rate of biodiesel with that of the alcohol blended fuels (almost similar oxidation reactivity rate) under low engine load, while the PM from biodiesel has higher oxidation reactivity rate than the PM from the alcohol blended fuels under high engine load. Also, DBM has the highest effect on the PM oxidation reactivity rate among the tested ternary fuels. This finding can support the results in micro and nano-structures of PM as mentioned before. Because the biodiesel has almost similar and higher effects on the PM micro and nano-structures parameters compared with the alcohol blended fuels under low and high load conditions, respectively, while DBM has the highest effect on the PM micro and nano-structures parameters among all the tested ternary fuels.

4. Conclusions

The present research aimed to explore the influence of various alternative fuels, including biodiesel, methanol, ethanol, butanol and pentanol, on the PM micro and nano-structures, volatility and oxidation reactivity from a CI engine under low (10%) and high (80%) engine loads. It is found that biodiesel and alcohols can significantly change the PM micro and nano-structures, volatility and oxidation reactivity compared to those of diesel fuel. The application of biodiesel and alcohol fuels causes in weaken the orderliness of the growth and accumulation process of the soot carbon layer, decrease in primary particle size (15% for biodiesel and about 7% for alcohols in average), fringe length (22.7% for biodiesel and about 16% for alcohols in average) and non-volatile substances, and increase in tortuosity (16.9% for biodiesel and about 13% for alcohols in average), volatile substances and oxidation reactivity rate, and almost no significant effect on fringe separation distance. The results show that these impacts of both biodiesel and alcohols on the parameters investigated are more obvious under the high engine load compared with the low engine load, while the pure biodiesel has the highest effect among all the tested alternative fuels.

CRediT author statement

Dongxu Mao: Conceptualization; Methodology; Investigation; Writing - Original Draft. Meisam Ahmadi Ghadikolaei: Methodology; Writing - Original Draft; Writing - Review & Editing. Chun Shun Cheung: Conceptualization; Methodology; Resources; Writing - Review & Editing; Supervision; Funding acquisition. Zhaojie Shen: Conceptualization; Methodology; Supervision. Wenzheng Cui: Conceptualization; Methodology; Supervision. Pak Kin Wong: Funding acquisition.

Declaration of competing interest

The authors declare that they have no known competing financial

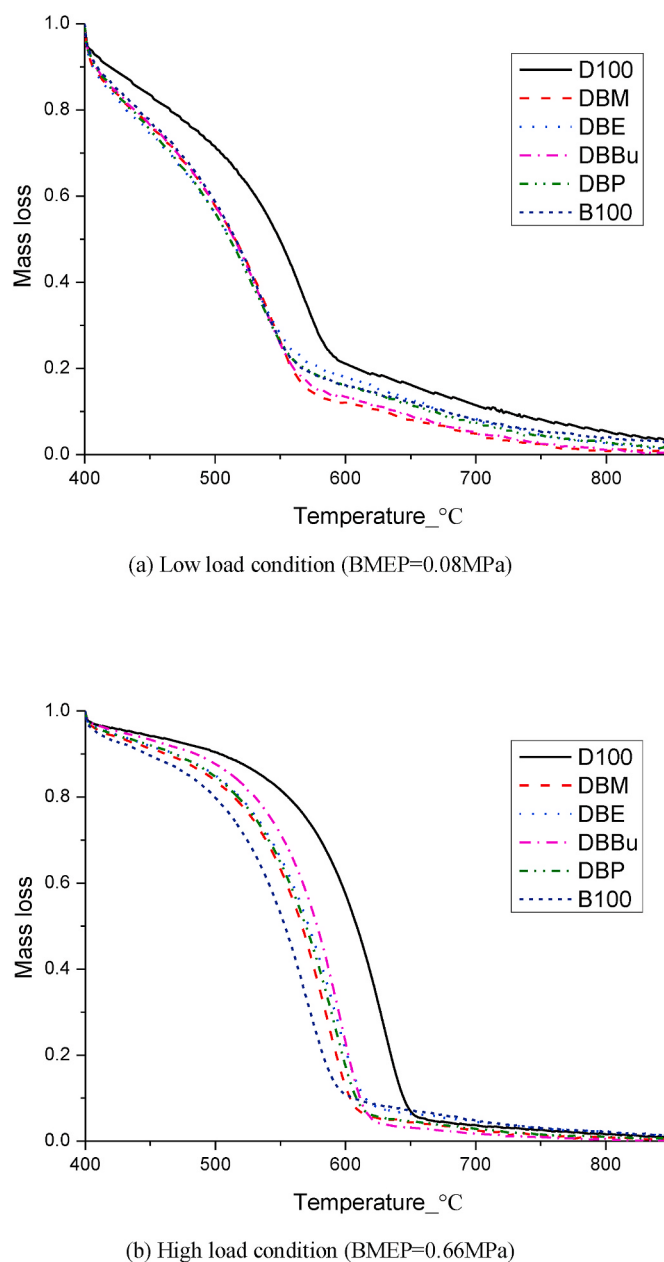


Fig. 9. Particle mass reduction curve of various fuels under low and high engine loads at 400–850 °C.

interests or personal relationships that could have appeared to influence the work reported in this paper.

Acknowledgements

The authors gratefully acknowledge the support of The Hong Kong Polytechnic University (Account No.: YBGD), National Natural Science Foundation of China (51606052), and Weihai Science and Technical Plan Project (2016DXGJMS10).

Nomenclature

•OH	Hydroxyl radical
ABE	Acetone-butanol-ethanol
B100	Biodiesel
BMEP	brake mean effective pressure
BP	Biodiesel-pentanol

D100	Diesel
DB	Diesel-biodiesel
DBBu	Diesel-biodiesel-butanol
DBE	Diesel-biodiesel-ethanol
DBM	Diesel-biodiesel-methanol
DBP	Diesel-biodiesel-pentanol
DBu	Diesel-butanol
D _s	Fringe separation distance
DSC	Differential scanning calorimeter
EC	Elemental carbon
GMD	Geometric mean diameter
L _a	Fringe length
OC	Organic carbon
PM	Particulate matter
ROI	Region of interest
SD	Standard deviation
SMPS	Scanning mobility particle sizer
STEM	Scanning transmission electron microscope
TEM	Transmission electron microscope
TEOM	Tapered element oscillating microbalance
T _f	Tortuosity
TGA	Thermogravimetric analyzer

References

- [1] Zhang ZH, Balasubramanian R. Effects of oxygenated fuel blends on the composition of size-segregated engine-out diesel particulate emissions and on the toxicity of quasi-ultrafine particles. *Fuel* 2018;215:161–70.
- [2] Cu M, Chen Y, Feng Y, Li C, Zheng J, Tian C, Yan C, Zhen M. Measurement of PM and its chemical composition in real-world emissions from non-road and on-road diesel vehicles. *Atmos Chem Phys* 2017;17:6779–95.
- [3] Shin SW, Song IH, Um SH. Role of physicochemical properties in nanoparticle toxicity. *Nanomaterials* 2015;5(3):1351–65.
- [4] Akhtar US, Rastogi N, McWhinney RD, Urch B, Chow CW, Evans GJ, Scott JA. The combined effects of physicochemical properties of size-fractionated ambient particulate matter on *in vitro* toxicity in human A549 lung epithelial cells. *Toxicology Reports* 2014;1:145–56.
- [5] Dockery DW, Pope CA, Xu X, Spengler JD, Ware JH, Fay ME, Ferris BG, Speizer FE. An association between air pollution and mortality in six U.S. Cities. *N Engl J Med* 1993;329:1753–9.
- [6] Gauderman WJ, Avol E, Gilliland F, Vora H, Thomas D, Berhane K, McConnell R, Kuenzli N, Lurmann F, Rappaport E, et al. The effect of air pollution on lung development from 10 to 18 years of age. *N Engl J Med* 2004;351:1057–67.
- [7] Katsouyanni K, Touloumi G, Samoli E, Gryparis A, Le Tertre A, Monopolis Y, Rossi G, Zmirou D, Ballester F, Boumghar A, et al. Confounding and effect modification in the short-term effects of ambient particles on total mortality: results from 29 European cities within the APHEA2 project. *Epidemiology* 2001;12(5):521–31.
- [8] Lee KO, Zhu J, Ciatti S, Yozgatligil A, Choi MY. Sizes, graphitic structures and fractal geometry of light-duty diesel engine particulates. *SAE Technical Paper* 2003. <https://doi.org/10.4271/2003-01-3169>. Paper No.:2003-01-3169.
- [9] Vander Wal RL, Tomasek AJ. Soot oxidation: dependence upon initial nanostructure. *Combust Flame* 2003;134(1–2):1–9.
- [10] Lu T, Cheung CS, Huang Z. Effects of engine operating conditions on the size and nanostructure of diesel particles. *J Aerosol Sci* 2012;47:27–38.
- [11] Zhu J, Lee KO, Yozgatligil A, Choi MY. Effects of engine operating conditions on morphology, microstructure, and fractal geometry of light-duty diesel engine particulates. *Proc Combust Inst* 2005;30(2):2781–9.
- [12] Vander Wal RL. Soot nanostructure: definition, quantification and implications. *SAE Technical Paper* 2005. <https://doi.org/10.4271/2005-01-0964>. Paper No: 2005-01-0964.
- [13] Müller JO, Su DS, Jentoft RE, Kröhnert J, Jentoft FC, Schlägl R. Morphology-controlled reactivity of carbonaceous materials towards oxidation. *Catal Today* 2005;102–103:259–65.
- [14] Su DS, Jentoft RE, Müller JO, Rothe D, Jacob E, Simpson CD, Tomović Ž, Müllen K, Messerer A, Pöschl U, et al. Microstructure and oxidation behaviour of Euro IV diesel engine soot: a comparative study with synthetic model soot substances. *Catal Today* 2004;90(1–2):127–32.
- [15] Yehliu K, Vander Wal RL, Armas O, Boehman AL. Impact of fuel formulation on the nanostructure and reactivity of diesel soot. *Combust Flame* 2012;159(12):3597–606.
- [16] Knauer M, Schuster ME, Su D, Schlägl R, Niessner R, Ivleva NP. Soot structure and reactivity analysis by Raman microspectroscopy, temperature-programmed oxidation, and high-resolution transmission electron microscopy. *J Phys Chem* 2009;113(50):13871–80.
- [17] Zhou JH, Cheung CS, Zhao WZ, Ning Z, Leung CW. Impact of intake hydrogen enrichment on morphology, structure and oxidation reactivity of diesel particulate. *Appl Energy* 2015;160:442–55.
- [18] Yesilyurt MK, Cesur C, Aslan V, Yilbasi Z. The production of biodiesel from safflower (*Carthamus tinctorius* L.) oil as a potential feedstock and its usage in compression ignition engine: a comprehensive review. *Renew Sustain Energy Rev* 2020;119:109574.
- [19] Yesilyurt MK, Aydin M, Yilbasi Z, Arslan M. Investigation on the structural effects of the addition of alcohols having various chain lengths into the vegetable oil-biodiesel-diesel fuel blends: an attempt for improving the performance, combustion, and exhaust emission characteristics of a compression ignition engine. *Fuel* 2020;269:117455.
- [20] Yesilyurt MK, Yilbasi Z, Aydin M. The performance, emissions, and combustion characteristics of an unmodified diesel engine running on the ternary blends of pentanol/safflower oil biodiesel/diesel fuel. *J Therm Anal Calorim* 2020;140:2903–42.
- [21] Zhen X, Wang Y, Liu D. Bio-butanol as a new generation of clean alternative fuel for SI (spark ignition) and CI (compression ignition) engines. *Renew Energy* 2020;147(1):2494–521.
- [22] Tian Z, Zhen X, Wang Y, Liu D, Li X. Combustion and emission characteristics of n-butanol-gasoline blends in SI direct injection gasoline engine. *Renew Energy* 2020;146:267–79.
- [23] Gong C, Li Z, Yi L, Huang K, Liu F. Research on the performance of a hydrogen/methanol dual-injection assisted spark-ignition engine using late-injection strategy for methanol. *Fuel* 2020;260:116403.
- [24] Gong C, Li Z, Yi L, Liu F. Experimental investigation of equivalence ratio effects on combustion and emissions characteristics of an H2/methanol dual-injection engine under different spark timings. *Fuel* 2020;262:116463.
- [25] Zhen X, Li X, Wang Y, Liu D, Tian Z. Comparative study on combustion and emission characteristics of methanol/hydrogen, ethanol/hydrogen and methane/hydrogen blends in high compression ratio SI engine. *Fuel* 2020;267:117193.
- [26] Gong C, Yi L, Zhang Z, Sun J, Liu F. Assessment of ultra-lean burn characteristics for a stratified-charge direct-injection spark-ignition methanol engine under different high compression ratios. *Appl Energy* 2020;261:114478.
- [27] Tian Z, Zhen X, Wang Y, Liu D, Li X. Comparative study on combustion and emission characteristics of methanol, ethanol and butanol fuel in TISI engine. *Fuel* 2020;259:116199.
- [28] Gong C, Zhang Z, Sun J, Chen Y, Liu F. Computational study of nozzle spray-line distribution effects on stratified mixture formation, combustion and emissions of a high compression ratio DISI methanol engine under lean-burn condition. *Energy* 2020;205:118080.
- [29] Ning L, Duan Q, Liu B, Zeng K. Experimental assessment of lean-burn characteristics for a modified diesel engine operated in methanol direct injection spark ignition (DISI) mode at full throttle condition. *Fuel* 2020;279:118455.
- [30] Gong C, Sun J, Liu F. Numerical study of twin-spark plug arrangement effects on flame, combustion and emissions of a medium compression ratio direct-injection methanol engine. *Fuel* 2020;279:118427.
- [31] Çelebi Y, Aydin H. An overview on the light alcohol fuels in diesel engines. *Fuel* 2019;236:890–911.
- [32] Chen H, Su X, He J, Xie B. Investigation on combustion and emission characteristics of a common rail diesel engine fueled with diesel/n-pentanol/methanol blends. *Energy* 2019;167:297–311.
- [33] Nayyar A, Sharma D, Soni SL, Bhardwaj B, Augustine M. Modeling and experimental investigation for performance and emissions on a diesel engine using bio-oxygenated ternary fuel blends. *Energy* 2019;168:136–50.
- [34] Ashok B, Jeevanantham AK, Nanthagopal K, Saravanan B, Kumar MS, Johny A, Mohan A, Kaisan MU, Abubakar S. An experimental analysis on the effect of n-pentanol-*Calophyllum Inophyllum* Biodiesel binary blends in CI engine characteristics. *Energy* 2019;173:290–305.
- [35] Nou M, Attia AMA, Sameh AN. Combustion, performance and emission analysis of diesel engine fuelled by higher alcohols (butanol, octanol and heptanol)/diesel blends. *Energy Convers Manag* 2019;185:313–29.
- [36] Ghadikolaei MA, Cheung CS, Yung KF. Study of combustion, performance and emissions of diesel engine fueled with diesel/biodiesel/alcohol blends having the same oxygen concentration. *Energy* 2018;157:258–69.
- [37] Wang X, Cheung CS, Di Y, Huang Z. Diesel engine gaseous and particle emissions fueled with diesel-oxygenate blends. *Fuel* 2012;94:317–23.
- [38] Kumar BR, Saravanan S, Rana D, Nagendran A. A comparative analysis on combustion and emissions of some next generation higher-alcohol/diesel blends in a direct-injection diesel engine. *Energy Convers Manag* 2016;119:246–56.
- [39] Yilmaz N, Atmanli A, Vigil FM. Quaternary blends of diesel, biodiesel, higher alcohols and vegetable oil in a compression ignition engine. *Fuel* 2018;212: 462–69.
- [40] Atmanli A. Comparative analyses of diesel waste oil biodiesel and propanol, n-butanol or 1-pentanol blends in a diesel engine. *Fuel* 2016;176:209–15.
- [41] Yilmaz N, Ileri E, Atmanli A. Performance of biodiesel/higher alcohols blends in a diesel engine. *Int J Energy Res* 2016;40:1134–43.
- [42] Imdadul HK, Masjuki HH, Kalam MA, Zulkifi NWM, Alabdulkarem A, Kamruzzaman M, Rashed MM. A comparative study of C4 and C5 alcohol treated diesel-biodiesel blends in terms of diesel engine performance and exhaust emission. *Fuel* 2016;179:281–8.
- [43] Tse H, Leung C, Cheung C. Performances, emissions and soot properties from a diesel-biodiesel ethanol blend fuelled engine. *Adv Automob Eng* 2016;S1:005. <https://doi.org/10.4172/2167-7670.S1-005>.
- [44] Tse H. Combustion and emissions of a diesel engine fueled with diesel-biodiesel-ethanol blends and supplemented with intake CO₂ charge dilution. In: Kyriacopoulou K, editor. *Developments in combustion technology*. London: Intech Open; 2016. p. 187–232.

- [45] Zhang ZH, Balasubramanian R. Physicochemical and toxicological characteristics of particulate matter emitted from a non-road diesel engine: comparative evaluation of biodiesel-diesel and butanol-diesel blends. *J Hazard Mater* 2014;264:395–402.
- [46] Luo J, Zhang Y, Wang J, Zhang Q. Effect of acetone-butanol-ethanol addition to diesel on the soot reactivity. *Fuel* 2018;226:555–63.
- [47] Zhu L, Xiao Y, Cheung CS, Guan C, Huang Z. Combustion, gaseous and particulate emission of a diesel engine fueled with n-pentanol (C5 alcohol) blended with waste cooking oil biodiesel. *Appl Therm Eng* 2016;102:73–9.
- [48] Fayad MA, Herreros JM, Martos FJ, Tsolakis A. Role of alternative fuels on particulate matter (PM) characteristics and influence of the diesel oxidation catalyst. *Environ Sci Technol* 2015;49:11967–73.
- [49] Fayad MA, Tsolakis A, Rodríguez DF, Herreros JM, Martos FJ, Lapuerta M. Manipulating modern diesel engine particulate emission characteristics through butanol fuel blending and fuel injection strategies for efficient diesel oxidation catalysts. *Appl Energy* 2017;190:490–500.
- [50] Ghadikolaei MA, Wei L, Cheung CS, Yung KP, Ning Z. Particulate emission and physical properties of particulate matter emitted from a diesel engine fueled with ternary fuel (diesel-biodiesel-ethanol) in blended and fumigation modes. *Fuel* 2020;263:116665.
- [51] Kline SJ, McClintock FA. Describing uncertainties in single sample experiments. *Mech Eng* 1953;75:3–8.
- [52] Tse H, Leung CW, Cheung CS. Investigation on the combustion characteristics and particulate emissions from a diesel engine fueled with diesel-biodiesel-ethanol blends. *Energy* 2015;83:343–50.
- [53] Zhang ZH, Tsang KS, Cheung CS, Chan TL, Yao CD. Effect of fumigation methanol and ethanol on the gaseous and particulate emissions of a direct-injection diesel engine. *Atmos Environ* 2011;45(11):2001–8.
- [54] Kumar BR, Saravanan S. Use of higher alcohol biofuels in diesel engines: a review. *Renew Sustain Energy Rev* 2016;60:84–115.
- [55] Jimenez S, Ballester J. A comparative study of different methods for the sampling of high temperature combustion aerosols. *Aerosol Sci Technol* 2005;39:811–21.
- [56] R'mili B, Bihan OLCL, Dutouquet C, Charriol OA, Frejaon E. Particle sampling by TEM grid filtration. *Aerosol Sci Technol* 2013;47:767–75.
- [57] Vargas AM, Gülder ÖL. A multi-probe thermophoretic soot sampling system for high-pressure diffusion flames. *Rev Sci Instrum* 2016;87(5). org/10.1063/1.4947509.
- [58] Lee J, Altman I, Choi M. Design of thermophoretic probe for precise particle sampling. *Aerosol Science* 2008;39:418–31.
- [59] Ogura I, Hashimoto N, Kotake M, Sakurai H, Kishimoto A, Honda K. Aerosol particle collection efficiency of holey carbon. *Aerosol Sci Technol* 2014;48:758–67.
- [60] Li Z, Qiu L, Cheng X, Li Y, Wu H. The evolution of soot morphology and nanostructure in laminar diffusion flame of surrogate fuels for diesel. *Fuel* 2018;211:517–28.
- [61] Yan F, Cheng X, Qiu L, Huang R, Huang S, Liu B. Spray flame soot sampling and morphology analysis of butanol-diesel blends. *J Energy Inst* 2017;90(6):855–63.
- [62] Zhang R, Kook S. Influence of fuel injection timing and pressure on in-flame soot particles in an automotive-size diesel engine. *Environ Sci Technol* 2014;48:8243–50.
- [63] Zhang R, Zhang Y, Kook S. Morphological variations of in-flame and exhaust soot particles associated with jet-to-jet variations and jet-jet interactions in a light-duty diesel engine. *Combust Flame* 2017;176:377–90.
- [64] Wang C, Chan QN, Kook S, Hawkes ER, Lee J, Medwell PR. External irradiation effect on the growth and evolution of in-flame soot species. *Carbon* 2016;102:161–71.
- [65] Su DS, Müller JO, Jentoft RE, Rothe D, Jacob E, Schlägl R. Fullerene-like soot from EURO-IV diesel engine: consequences for catalytic automotive pollution control. *Top Catal* 2004;30(1–4):241–5.
- [66] Rohani B, Bae C. Morphology and nano-structure of soot in diesel spray and in engine exhaust. *Fuel* 2017;203:47–56.
- [67] Kirchner U, Scheer V, Vog R, Kagi R. TEM study on volatility and potential presence of solid cores in nucleation mode particles from diesel powered passenger cars. *Aerosol Science* 2009;40:55–64.
- [68] Mathis U, Kaegi R, Mohr M, Zenobi R. TEM analysis of volatile nanoparticles from particle trap equipped diesel and direct-injection spark-ignition vehicles. *Atmos Environ* 2004;38:4347–55.
- [69] Salamanca M, Mondragón F, Agudelo JR, Santamaría A. Influence of palm oil biodiesel on the chemical and morphological characteristics of particulate matter emitted by a diesel engine. *Atmos Environ* 2012;62:220–7.
- [70] Qu L, Wang Z, Zhang J. Influence of waste cooking oil biodiesel on oxidation reactivity and nanostructure of particulate matter from diesel engine. *Fuel* 2016;181:389–95.
- [71] Vander Wal RL, Yezzerets A, Currier NW, Kim DH, Wang CM. HRTEM Study of diesel soot collected from diesel particulate filters. *Carbon* 2007;45:70–7.
- [72] Soriano JA, Agudelo JR, López AF, Armas O. Oxidation reactivity and nanostructural characterization of the soot coming from farnesane - a novel diesel fuel derived from sugar cane. *Carbon* 2017;125:516–29.
- [73] Yang H, Li X, Wang Y, Mu M, Li X, Kou G. Experimental investigation into the oxidation reactivity and nanostructure of particulate matter from diesel engine fuelled with diesel/polyoxymethylene dimethyl ethers blends. *Sci Rep* 2016;6. <https://doi.org/10.1038/srep37611>.
- [74] Bérubé KA, Jones TP, Williamson BJ, Winters C, Morgan AJ, Richards RJ. Physicochemical characterisation of diesel exhaust particles: factors for assessing biological activity. *Atmos Environ* 1999;33(10):1599–614.
- [75] Fierz M, Kaegi R, Burtscher H. Theoretical and experimental evaluation of a portable electrostatic TEM sampler. *Aerosol Sci Technol* 2007;41(5):520–8.
- [76] Yehliu K, Vander Wal RL, Boehman AL. Development of an HRTEM image analysis method to quantify carbon nanostructure. *Combust Flame* 2011;158(9):1837–51.
- [77] Wal RLV, Tomasek AJ, Pamphlet MI, Taylor CD, Thompson WK. Analysis of HRTEM images for carbon nanostructure quantification. *J Nanoparticle Res* 2004;6 (6):555–68.
- [78] Gargiulo V, Alfè M, Blasio GD, Beatrice C. Chemico-physical features of soot emitted from a dual-fuel ethanol-diesel system. *Fuel* 2015;150:154–61.
- [79] Ghadikolaei MA, Yung KP, Cheung CS, Ho SSH, Wong PK. Non-polar organic compounds, volatility and oxidation reactivity of particulate matter emitted from diesel engine fueled with ternary fuels in blended and fumigation modes. *Chemosphere* 2020;249:126086.
- [80] Lu T, Cheung CS, Huang Z. Investigation on particulate oxidation from a DI diesel engine fueled with three fuels. *Aerosol Sci Technol* 2012;46(12):1349–58.
- [81] Wei L, Cheung CS, Ning Z. Influence of waste cooking oil biodiesel on the nanostructure and volatility of particles emitted by a direct-injection diesel engine. *Aerosol Sci Technol* 2016;50(9):893–905.
- [82] Mao D, Cheung CS, Shen Z, Cui W. Study on the difference of combustion and emission characteristics of alcoholic fuels with same oxygen content. *Chin Intern Combust Engine Eng* 2019;40(2):16–21.
- [83] Meißner J, Pasel J, Peters R, Samsun RC, Tschauder A, Stolten D. Elimination of by-products of autothermal diesel reforming. *Chem Eng J* 2016;306:107–16.
- [84] Bu J, Loh G, Gwie CG, Dewiyanti S, Tasrif M, Borgna A. Desulfurization of diesel fuels by selective adsorption on activated carbons: competitive adsorption of polycyclic aromatic sulfur heterocycles and polycyclic aromatic hydrocarbons. *Chem Eng J* 2011;166(1):207–17.
- [85] Ballesteros R, Hernández JJ, Lyons LL, Cabañas B, Tapia A. Speciation of the semivolatile hydrocarbon engine emissions from sunflower biodiesel. *Fuel* 2008;87 (10–11):1835–43.
- [86] Li X, Xu Z, Guan C, Huang Z. Particle size distributions and OC, EC emissions from a diesel engine with the application of in-cylinder emission control strategies. *Fuel* 2014;121:20–6.